Influence of carbon deposits on the cobalt-catalyzed Fischer-Tropsch reaction: evidence of a two-site reaction model

ACS Catalysis

Research Article

pubs.acs.org/acscatalysis

Influence of Carbon Deposits on the Cobalt-Catalyzed Fischer–Tropsch Reaction: Evidence of a Two-Site Reaction Model

Wei Chen,[†] Tobias F. Kimpel,[†] Yuanjun Song,[‡] Fu-Kuo Chiang,[§] Bart Zijlstra,[†] Robert Pestman,[†] Peng Wang,[†,§] and Emiel J. M. Hensen*[,†]

[†]Laboratory of Inorganic Materials Chemistry, Schuit Institute of Catalysis, Department of Chemical Engineering and Chemistry, Eindhoven University of Technology, P.O. Box 513, 5600 MB Eindhoven, The Netherlands

[‡]Beijing Key Laboratory for Magneto-Photoelectrical Composite and Interface Science, School of Mathematics and Physics, University of Science and Technology Beijing, Beijing 100083, People's Republic of China

[§]National Institute of Clean-and-Low-Carbon Energy, Shenhua Group, Shenhua NICE, Future Science & Technology City, Changping District, Beijing 102211, People's Republic of China

ABSTRACT: One of the well-known observations in the Fischer–Tropsch (FT) reaction is that the CH_4 selectivity for cobalt catalysts is always higher than the value expected on the basis of the Anderson–Schulz–Flory (ASF) distribution. Depositing graphitic carbon on a cobalt catalyst strongly suppresses this non-ASF CH_4, while the formation of higher hydrocarbons is much less affected. Carbon was laid down on the cobalt catalyst via the Boudouard reaction. We provide evidence that the amorphous carbon does not influence the FT reaction, as it can be easily hydrogenated under reaction conditions. Graphitic carbon is rapidly formed and cannot be removed. This unreactive form of carbon is located on terrace sites and mainly decreases the CO conversion by limiting CH_4 formation. Despite nearly unchanged higher hydrocarbon yield, the presence of graphitic carbon enhances the chain-growth probability and strongly suppresses olefin hydrogenation. We demonstrate that graphitic carbon will slowly deposit on the cobalt catalysts during CO hydrogenation, thereby influencing CO conversion and the FT product distribution in a way similar to that for predeposited graphitic carbon. We also demonstrate that the buildup of graphitic carbon by ^{13}CO increases the rate of C–C coupling during the $^{12}C_3H_6$ hydrogenation reaction, whose products follow an ASF-type product distribution of the FT reaction. We explain these results by a two-site model on the basis of insights into structure sensitivity of the underlying reaction steps in the FT mechanism: carbon formed on step-edge sites is involved in chain growth or can migrate to terrace sites, where it is rapidly hydrogenated to CH_4. The primary olefinic FT products are predominantly hydrogenated on terrace sites. Covering the terraces by graphitic carbon increases the residence time of CH_x intermediates, in line with decreased CH_4 selectivity and increased chain-growth rate.

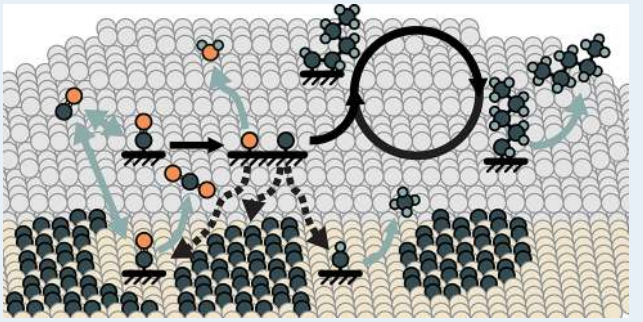

KEYWORDS: *Fischer–Tropsch, cobalt, methane, two-site model, carbon deposits*

1. INTRODUCTION

Since Fischer–Tropsch (FT) synthesis was discovered in 1925,[1,2] this fascinating reaction has attracted tremendous interest from chemists and chemical engineers.[3,4] Today, it has been commercialized for the conversion of cheap coal and natural gas feedstock to a variety of products, including clean transportation fuels and chemicals.[5−7] Given the abundance and low price of natural gas in certain areas, CH_4 is preferred over coal for the production of synthesis gas. In addition, synthesis gas production, which accounts for 60–70% of the capital and running costs of a typical FT plant,[7] is cheaper with CH_4 as the feedstock. A central issue in commercial FT technology is to minimize the production of CH_4, which has the lowest value among the hydrocarbon products.

The main products of cobalt-catalyzed FT synthesis are linear olefins and paraffins.[8] A typical hydrocarbon distribution is strongly reminiscent of the Anderson–Schulz–Flory (ASF) distribution, which is typically found for the products of oligomerization or polymerization processes.[9,10] The CH_4 selectivity on cobalt is always higher than the ideal ASF distribution on the basis of higher hydrocarbons predictions. This observation has been attributed to thermodynamically favored formation of CH_4, since the bond strength of C–H in CH_4 (435 kJ mol^{-1}) is higher than that of the C–C bond (376 kJ mol^{-1} in ethane).[8] The deviation in CH_4 selectivity has also been explained by facile hydrogenation of the surface CH_x to CH_4 in comparison to hydrogenation of surface intermediates to higher hydrocarbons.[11] However, recent simulations using a

Received: October 24, 2017
Revised: December 7, 2017
Published: December 15, 2017

DOI: 10.1021/acscatal.7b03639
ACS Catal. XXXX, XXX, XXX−XXX

reversible chain-growth model show that increasing the rate constant of CH_x hydrogenation does not lead to a lower propagation rate for CH_x but rather to a lower chain-length-independent chain-growth probability.[12] In addition to the metallic phase in the catalyst, the support material influences the methane formation as well. Prieto et al. reported that the methane selectivity is at a maximum as a function of the acid−basic character of the support, and that a highly basic dopant such as SmO_x can suppress methane formation.[13]

A thorough understanding of the formation of CH_4 in the FT process is fundamentally important to improve the performance of cobalt catalysts. Modern computational approaches combined with the development of accurate nanoparticle model systems enable an in depth study of this issue, in which a knowledge of structure sensitivity plays a key role.[14,15] It is widely documented that the dissociation of diatomic molecules with π bonds such as CO,[16,17] NO,[18,19] and N_2[20] preferably takes place on step-edge sites. Whereas this is well accepted for N_2 dissociation in the context of ammonia synthesis,[21] there is less agreement on the mode of CO dissociation under FT conditions.[22,23] Direct CO dissociation is preferred on step edges over terraces.[22] The main alternative idea is that CO can be dissociated in an H-assisted manner: i.e., involving HCO[24,25] or HCOH[26,27] as intermediates. Chain growth has also been compared on step edges and terrace sites. Cheng et al. reported that the lowest energy barrier of CH_x−CH_y bond formation involves CH_2 + CH_2 reactions, which are strongly favored on a stepped cobalt surface in comparison to a flat surface.[28] In contrast, CH_x hydrogenation, in which a σ-bond is formed, is usually regarded as a structure-insensitive reaction.[14,15] As CH_x binds more weakly on a terrace in comparison to a stepped surface, one expects slightly fast CH_x hydrogenation on terraces.[29] Related to this, the hydrogenation of growing hydrocarbon chains on the catalytic surface is also assumed to be independent of the surface topology.[14,15] A microkinetic model that compares different mechanisms for the FT reaction on a stepped Ru surface showed that hydrocarbons are mainly obtained via direct CO dissociation; CR + CH type coupling reactions mainly produce olefins as the primary products.[30] A hypothesis derived from these insights is that part of the (non-ASF) CH_4 is obtained on terrace sites. However, direct evidence for this speculation is lacking.

Carbon can be deposited on the surface in different forms and is considered to be one of the causes of catalyst deactivation.[31] It has been established that amorphous carbon and less structured carbon deposits can reversibly transform into graphitic carbon, which kinetically and thermodynamically prefers the flat surface of cobalt over the stepped surface.[32−36] Accordingly, this makes it possible to selectively block the flat surface by the Boudouard reaction ($2CO \rightarrow C + CO_2$), assuming that amorphous carbon can be easily removed. We have previously shown that CO disproportionation via the Boudouard reaction is a structure-sensitive reaction.[37] It occurs at a high rate in the absence of H_2 but suffers from rapid deactivation due to the buildup of carbon. In the present work, we characterize in more detail the carbon species deposited during the Boudouard reaction and their propensity toward hydrogenation. In this way, we found that amorphous carbon can be removed by hydrogenation at intermediate temperature, retaining the graphitic carbon. In this way, we could investigate the impact of graphitic carbon on the FT reaction, as well as the H_2/C_3H_6 reaction. The reaction data will be discussed in terms of a two-site model involving step-edge sites for CO dissociation, chain growth, and termination, while the terrace sites are involved in CH_4 formation. Blocking the latter sites by graphitic carbon suppresses CH_4 formation. The concomitant increase in chain-growth probability is explained by the suppressed migration of CH_x intermediates from the step-edge sites to terrace sites.

2. EXPERIMENTAL SECTION

2.1. Preparation and Basic Characterization. The Co/SiO_2 catalyst containing 17.1 wt % Co and 0.04 wt % Pt (ICP-OES, Spectroblue, Ametek Inc.) was prepared by incipient wetness impregnation of a silica support (120−250 μm, provided by Shell) using an aqueous solution of $Co(NO_3)_2 \cdot 6H_2O$ (99.99%, Merck) and $Pt(NH_3)_4 \cdot (NO_3)_2$ (99.995%, Alfa Aesar) as precursors. The detailed preparation of this catalyst can be found in the literature.[37] The accessible surface area of 116.7 μmol of Co atoms/g of catalyst was determined by H_2-chemisorption (ASAP 2010, Micromeritics). The average cobalt particle size of 15 nm was determined by TEM analysis (FEI Tecnai 20) and confirmed by in situ XRD (D/max-2600, Rigaku).

2.2. Carbon Deposition and Temperature-Programmed Hydrogenation. Carbon deposition and subsequent temperature-programmed hydrogenation (TPH) were performed in a tubular reactor. Typically, 200 mg of the Co/SiO_2 catalyst was reduced in situ in a dilute H_2 flow (20% H_2 in Ar, 50 mL min^{-1} in total) at 450 °C (heating rate of 2 °C min^{-1}) and atmospheric pressure for 16 h and subsequently flushed in an Ar flow for 2 h. Then, the reactor was cooled to the desired carbon deposition temperature. Carbon was deposited by exposure to a diluted CO flow (10% CO in Ar, 50 mL min^{-1} in total). After deposition, the catalyst was flushed in Ar for 2 h and cooled to room temperature. The TPH experiments were conducted by heating the reactor to 550 °C at a rate of 5 °C min^{-1} under an H_2 flow (10% H_2 in Ar, 50 mL min^{-1} in total). The main hydrocarbon product of carbon hydrogenation was CH_4, as followed by an online mass spectrometer (ESS, GeneSys Evolution). To determine the exact CH_4 flow rate, the mass spectrometer (MS) signal was calibrated using a known gas mixture. The amount of predeposited carbon was determined by integrating the CH_4 flow with time on stream.

2.3. Quasi in Situ X-ray Photoelectron Spectroscopy. Carbon deposition on the Co/SiO_2 catalyst was studied by quasi in situ XPS using a Kratos AXIS Ultra 600 spectrometer equipped with a monochromatic Al Kα X-ray source (Al Kα energy is 1486.6 eV). Survey scans were recorded at pass energies of 160 and 40 eV for detailed region scans. The step size was 0.1 eV in both cases, and the background pressure during the experiment was kept below 5×10^{-6} mbar. A high-temperature reaction cell (Kratos, WX-530) was used to pretreat the sample, which was supported on an alumina stub, allowing in vacuo sample transfer into the XPS measurement chamber.

The initial reduction was performed in a 50% H_2 in Ar flow at atmospheric pressure and 450 °C for 8 h. After reduction the sample was cooled to 150 °C and subsequently transferred to the measurement chamber. For the carbon deposition, the sample was heated in a flow of 50 mL of Ar to 260 °C at a rate of 5 °C min^{-1}. As soon as the target temperature was reached, the gas flow was switched to a flow of 20% CO in Ar. After the desired carbon deposition time, the gas flow was stopped and

DOI: 10.1021/acscatal.7b03639
ACS Catal. XXXX, XXX, XXX−XXX

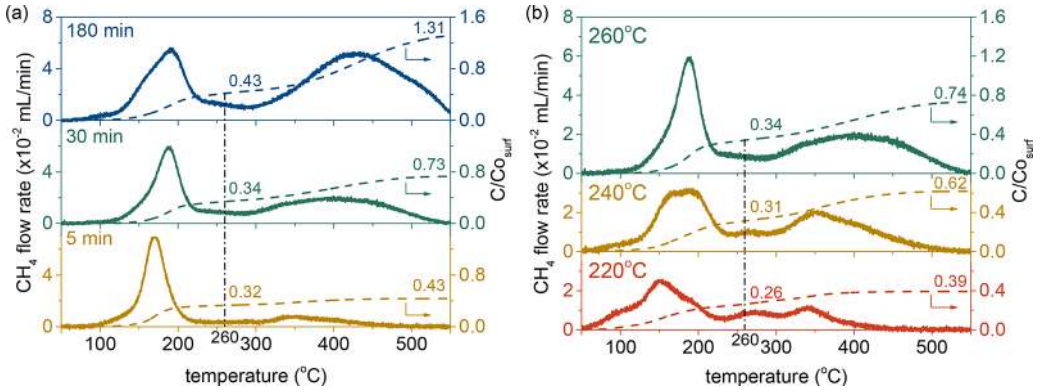

Figure 1. TPH profiles of the carbon deposits obtained by CO exposure at 260 °C for different times (a) and at different temperatures for 30 min (b). The amount of carbon was quantified by integrating the CH_4 flow.

the reaction cell was immediately evacuated and cooled to room temperature. Energy calibration was done using the Co $2p_{3/2}$ peak at 778.2 eV for the reduced samples and the Si 2s peak at 103.3 eV of the SiO_2 support for the calcined sample.

2.4. Environmental Transmission Electron Microscopy. Environmental transmission electron microscopy (TEM) images were recorded on a FEI ETEM instrument at an acceleration voltage of 300 kV. A ground sample was reduced in situ at 450 °C in a NanoEx-i/v sample holder capable of heating. The reduced sample was exposed to CO gas (12 mbar) at 260 °C for 1.5 h. TEM images were taken at room temperature under vacuum.

2.5. Catalytic Activity Measurements. Steady-state and transient catalytic activity measurements were performed in a setup that is capable of switching gas feeding. After reduction at 450 °C for 16 h, the reactor was cooled to the desired temperature (220 or 260 °C) in an Ar flow and an increase in the pressure to 2 bar. The flow was subsequently switched to a synthesis gas mixture ($CO/H_2/Ar$). The partial pressures of H_2 and CO were adjusted by varying their flow rates. The total flow rate was fixed at 50 mL min^{-1} by using Ar as balance. The activity and selectivity were measured by online analysis with a VARIAN CP-3800 gas chromatograph equipped with FID and TCD for analysis of hydrocarbon and permanent gases, respectively.

To study the reactivity of predeposited carbon, a diluted ^{13}CO flow (10% ^{13}CO in Ar, 50 mL min^{-1} in total) was used to deposit isotopically labeled carbon at 260 °C for 30 min. Afterward, the ^{13}CO flow was replaced by an Ar flow to remove molecularly adsorbed ^{13}CO. After flushing with Ar for 2 h, the Ar flow was abruptly switched to a $^{12}CO/H_2$ feed. The transient responses of H_2 (m/z 2), $^{12}CH_4$ (m/z 15), $^{13}CH_4$ (m/z 17), ^{12}CO (m/z 28), and ^{13}CO (m/z 29) were monitored by online mass spectrometry.

Steady-state isotopic transient kinetic analysis (SSITKA) was performed by switching from $^{12}CO/H_2/Ar$ to $^{13}CO/H_2/Ne$ when steady-state conversion was obtained, in which the Ne was used as a tracer to determine the gas-phase hold-up time. Procedures to determine the residence time and coverages of CO and CH_x (intermediates of CH_4) are provided in our earlier work.[38]

3. RESULTS

3.1. Carbon Deposition by CO Exposure. In order to study the influence of surface carbon deposits on the CO hydrogenation reaction, carbon was deposited by the Boudouard reaction ($2CO \rightarrow CO_2 + C$) on reduced Co/SiO_2. We employed TPH to determine the reactivity of the deposited carbon species. Figure 1 shows TPH traces as a function of the carbon deposition time and the carbon deposition temperature. We distinguish two types of carbon species. The first type of deposited carbon can be hydrogenated below 260 °C. Accordingly, we can assign these carbon species to atomic carbon or amorphous carbon on the basis of the literature.[33,35,39,40] As the temperature at which these amorphous carbon species can be hydrogenated is in the FT reaction regime (200−240 °C), these carbon species are most likely involved in the FT reaction. Figure 1a shows that the amount of the less reactive carbon increases strongly during prolonged CO exposure. H_2-chemisorption data reported in Table 1 compare the metallic cobalt surface area of freshly reduced Co/SiO_2 with samples exposed to CO and subsequently reduced at 260 °C to remove most of the reactive carbon species. Clearly, the deposition of carbon species causes a strong decrease in the metallic cobalt surface area. CO exposure at 260 °C for 3 h decreases the surface that can be probed by H_2 chemisorption by about 95%.

Table 1. Cobalt Surface Area Measured by H_2 Chemisorption[a]

CO exposure	Co surface (m^2 g_{Co}^{-1})	relative loss (%)	C_{graph}/Co_{surf}[b]
	30.4		
200 °C, 30 min	29.8	2	
220 °C, 30 min	22.5	26	0.13
260 °C, 30 min	18.5	39	0.39
260 °C, 3 h	1.4	95	0.98

[a]The carbon-predeposited catalysts were exposed to a H_2 flow for 6 h at 260 °C before the H_2-chemisorption measurement. [b]C_{graph}/Co_{surf} determined by integration of the CH_4 signal above 260 °C during TPH (cf. Figure 1).

We also characterized these carbon species by XPS. For this purpose, we carried out similar carbon deposition experiments on an in situ reduced Co/SiO_2 catalyst in a reaction chamber directly attached to an XPS spectrometer. A highly oriented pyrolytic graphite reference was used to fit the sp^2 carbon in C 1s spectra.[41] Figure 2 (left) shows that this procedure leads to sp^2 and sp^3 carbon species as follows from the C 1s states at 284 and 285 eV, respectively.[41] The amount of sp^2 carbon increases with CO exposure time. Exposure of the carbon deposits to H_2 at 260 °C results in a decrease of the amount of

DOI: 10.1021/acscatal.7b03639
ACS Catal. XXXX, XXX, XXX−XXX

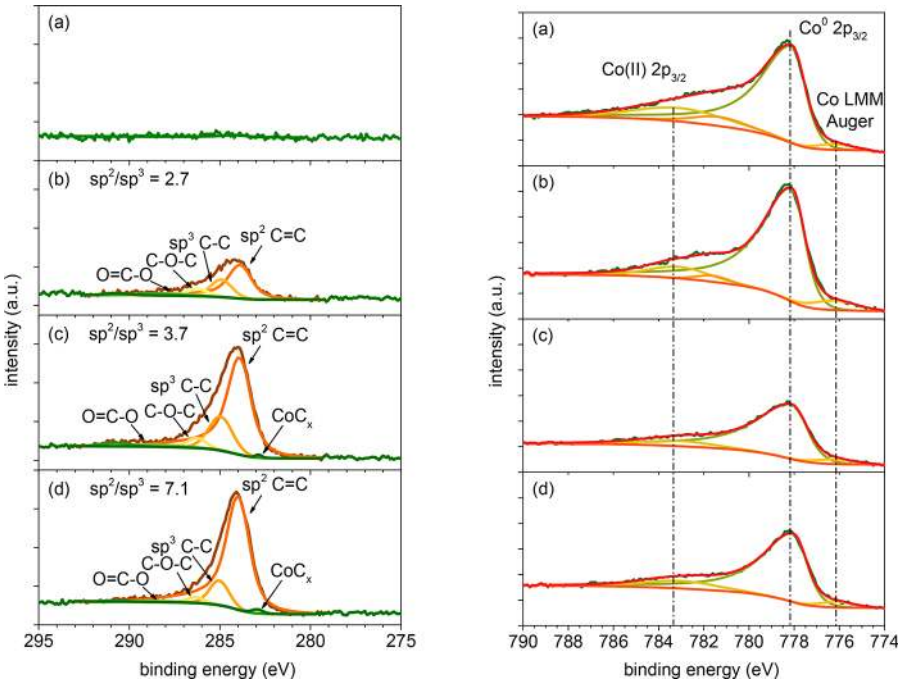

Figure 2. Quasi in situ XPS spectra of the C 1s regions (left) and Co 2p regions (right) of the Co/SiO_2 catalyst: after reduction at 450 °C (a), subsequent CO exposure at 260 °C for 30 min (b) and 4 h (c), and finally hydrogenation at 260 °C for 5 min (d).

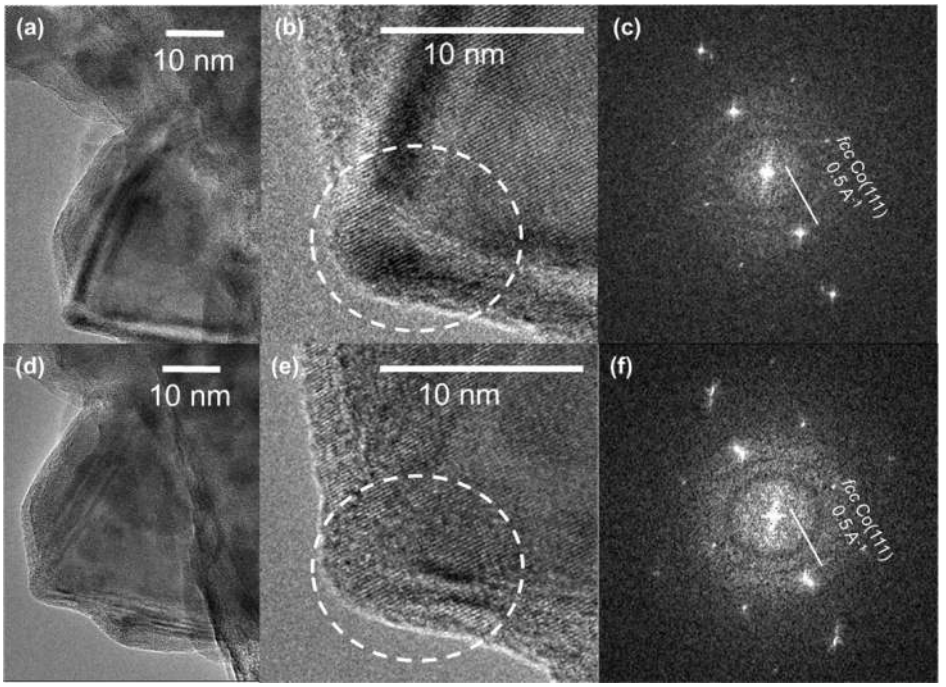

Figure 3. Environmental TEM images and fast Fourier transform patterns of selected areas of a cobalt nanoparticle in the *in situ* reduced Co/SiO_2 catalyst before (a–c) and after (d–f) CO exposure at 260 °C (12 mbar, 80 min).

sp^3 carbon, while the intensity of sp^2 carbon remains nearly unchanged. This result highlights the low reactivity of sp^2 carbon. XPS quantification shows that about 88% of the carbon species after 4 h of CO exposure at 260 °C is sp^2 carbon. As hexagonal graphite, primarily consisting of sp^2 carbon, is commensurate with the hexagonal close-packed surface of cobalt terraces,[40,42] we conclude that the less reactive carbon is graphitic. The contribution of carbidic carbon (282.9 eV[40,43,44]) after 4 h of CO exposure at 260 °C is below 1%. XPS spectra of the Co 2p region are presented in Figure 2. An asymmetric peak shape was used to fit the metallic cobalt component.[45] An Al Kα excited cobalt $L_2M_{23}M_{45}$ Auger transition at 776.2 eV (2.2 eV fwhm) was added in the fitting procedure.[45,46] The spectra do not contain evidence for the formation of cobalt carbide, as the Co 2p binding energy of cobalt carbide[47,48] is 0.4–0.6 eV lower than that of metallic Co (278.1 eV[45]). Environmental TEM images (Figure 3) of a cobalt particle before and after 80 min exposure to 12 mbar of

DOI: 10.1021/acscatal.7b03639
ACS Catal. XXXX, XXX, XXX–XXX

CO at 260 °C do not show a significant change in the metallic cobalt structure, confirming that formation of cobalt carbide can be excluded. The formation of a carbon adlayer on the cobalt particle cannot be clearly seen from these environmental TEM measurements, although the diffraction pattern in the fast Fourier transform of the selected area suggest the formation of an amorphous layer on the surface. It has been shown before that CO exposure at much higher temperature leads to formation of multilayered graphitic carbon enwrapping the cobalt particle.[49]

We also studied carbon deposition at lower temperature. After CO exposure at 220 °C (Figure 1b), the TPH profile shows the presence of multiple carbon species below 260 °C. Moreover, a much lower amount of graphitic carbon is formed in comparison to samples exposed to CO at 260 °C. One can also see that the total amount of amorphous carbon is much less affected by the deposition temperature and deposition time in comparison to the amount of graphitic carbon. This suggests that the more reactive amorphous carbon species are the primary products of CO dissociation and that these species are slowly converted into a more stable graphitic form.[33−36] It has been reported that the transformation between these carbon species is reversible.[33]

Quantifying the deposited carbon reveals that the amount of amorphous carbon does not change markedly, either with the carbon deposition time (Figure 1a) or with the carbon deposition temperature (Figure 1b). This is in keeping with a surface science study by Nakamura et al., who investigated carbon deposition on a polycrystalline cobalt foil.[34] Accordingly, we speculate that this type of carbon is closely associated with surface cobalt sites involved in CO activation. Considering the absence of H_2 during carbon deposition, it is likely that step edges are the active sites for CO dissociation.[50,51] In a recent study, we also emphasized the importance of a minority site on the surface involved in direct CO dissociation.[37] In the absence of H_2, the O atoms can only be removed as CO_2, leading to the predominant coverage of the cobalt surface with carbon. Because of the low diffusion barrier, i.e. 26 kJ mol^{-1} on Co(0001),[42,52] carbon atoms can easily migrate over the cobalt surface and form agglomerates of carbon atoms through C−C coupling reactions on terraces. Additional DFT calculations estimate the migration barrier for diffusion of a C atom from the 4-fold step-edge site to the terrace to be 75 kJ mol^{-1}.[30] Coupling between C atoms is much easier on terraces than on steps with respective activation barriers of 118 and 234 kJ mol^{-1}, respectively.[32] Formation of (poly)aromatic structures containing predominantly sp^2 carbon can explain the low reactivity of these deposits.[42] It has also been reported that the hexagonal graphite structure is thermodynamically favorable on the close-packed surface.[40,42] Figure 1b clearly shows that the formation of graphitic carbon is facilitated by higher CO exposure temperature.[34,35] We therefore conclude that the graphitic carbon formed via CO exposure mainly covers the terrace sites that dominate the surface of the relatively large cobalt nanoparticles in Co/SiO_2. Furthermore, the step-edge sites will also contain a variety of carbon species, which are likely CH_x species.

The reactivity of the carbon deposits is demonstrated in Figure 4, where a $^{12}CO/H_2$ flow is passed over the ^{13}C-precovered Co/SiO_2 catalyst. The transient response shows that $^{13}CH_4$ appears concomitantly with H_2, demonstrating the involvement of predeposited ^{13}C in $^{13}CH_4$ formation at 260 °C. ^{12}CO adsorption and hydrogenation cannot proceed until a certain amount of free sites is regenerated by ^{13}C hydrogenation. This causes a 1.5 s delay (corrected for the chromatographic effect of CO) of $^{12}CH_4$ formation in comparison to $^{13}CH_4$ formation. Taking into account the TPH profile in Figure 1 and quantifying the amount of $^{13}CH_4$ formed, we find that a part of the reactive ^{13}C deposits is hydrogenated to $^{13}CH_4$ after the switch to a H_2-containing feed. The remainder of the ^{13}C species, mainly in the form of graphitic carbon, stays on the surface. The influence of these residual carbon deposits on the catalyst under model FT conditions will be discussed below.

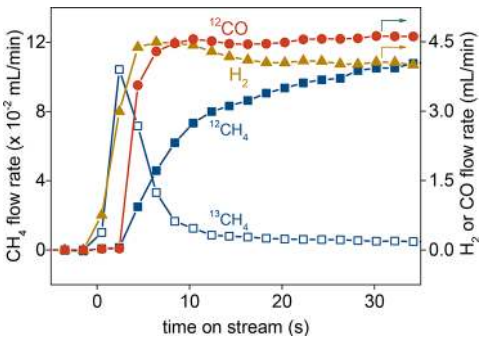

Figure 4. Transient responses of $^{13}CH_4$ (open squares), $^{12}CH_4$ (solid squares), ^{12}CO (circles), and H_2 (triangles) following an Ar → $^{12}CO/H_2$ switch over a ^{13}C-precovered Co/SiO_2 catalyst obtained by ^{13}CO exposure at 260 °C for 30 min followed by Ar flushing for 2 h (conditions: ρ_{H_2} = 200 mbar, ρ_{CO} = 200 mbar, T = 260 °C).

3.2. Influence of Carbon Deposits on the CO Hydrogenation Reaction.

As confirmed by Figure 1a, the amount of the graphitic carbon strongly increases with the carbon deposition time. In this way, we can study the CO hydrogenation reaction on cobalt catalysts that are precovered with different amounts of graphitic carbon. The resulting data are reported in Figure 5. The catalytic performance is plotted as a function of graphitic carbon to surface cobalt ratio (denoted as C_{graph}/Co_{surf}). C_{graph} relates to the amount of carbon hydrogenated above 260 °C in separate TPH experiments. All of the data in Figure 5 were obtained after 6 h time on stream under model FT reaction conditions. The model FT reactions were carried out at 260 and 220 °C and a H_2/CO ratio of 1.

We first verified whether amorphous carbon influences the catalytic performance. The open symbols in Figure 5a represent the experiment in which CO exposure at 260 °C for 30 min was followed by hydrogenation at 260 °C for 2 h in order to remove most of the amorphous carbon. The resulting reaction data are nearly identical with those obtained without the hydrogenation step at 260 °C, demonstrating that predeposited amorphous carbon does not influence the FT performance. This is expected, as most of the amorphous carbon can be easily removed below 260 °C in a TPH experiment (Figure 1). This leads to the conclusion that the effect of carbon deposition on the model FT reaction at 260 °C to be discussed below is mainly exerted by the presence of graphitic carbon.

Figure 5a,b reveals that the presence of graphitic carbon decreases the CO consumption rate under both reaction conditions. The activity decrease is more evident at 260 °C than at 220 °C. Strikingly, these data also show that graphitic carbon affects the formation rates of different products in

DOI: 10.1021/acscatal.7b03639
ACS Catal. XXXX, XXX, XXX−XXX

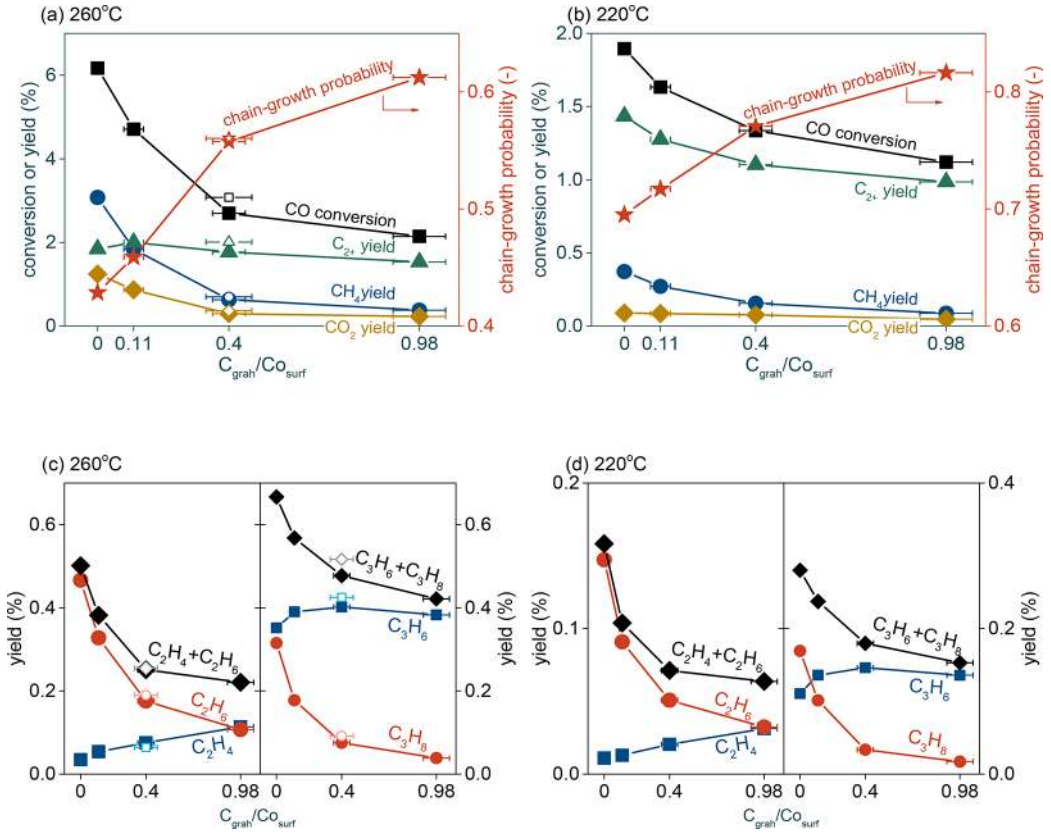

Figure 5. Catalytic properties of the FT reaction over carbon-precovered Co/SiO_2 as a function of graphitic carbon to surface cobalt ratio (denoted as C_{graph}/Co_{surf}): (a, b) CO conversion (squares), CH_4 yield (circles), C_{2+} yield (triangles), CO_2 yield (diamonds), and chain-growth probability (stars, based on C_3−C_6 hydrocarbons); (c, d) C_2 (left) and C_3 products (right) yields. Conditions: ρ_{H_2} = 200 mbar, ρ_{CO} = 200 mbar, T = 260 °C (a, c) and 220 °C (b, d). The error bars present the systematic error introduced by the carbon quantification that is done by integrating the TPH profiles on a calibrated online MS.

profoundly different ways. While the decrease in CO consumption rate is accompanied by a substantial decrease in the CH_4 yield, the yield of C_{2+} hydrocarbon products (paraffins and olefins containing two or more carbon atoms) remains nearly the same. In addition, the chain-growth probability (based on C_3−C_6 hydrocarbons) increases with the graphitic carbon content of the precovered catalyst. At 260 °C, the chain-growth probability increases from 0.43 for the clean cobalt surface to 0.61 for the nearly completely poisoned cobalt surface. When the reaction is carried out at 220 °C, the chain-growth probability also changes from 0.70 to 0.82 due to the presence of graphitic carbon. Concomitant with the decrease in CH_4 yield, we see that the CO_2 yield is decreased for both cases. Clearly, these data show that partial poisoning of the cobalt surface by graphitic carbon substantially inhibits CO conversion as well as CH_4 and CO_2 formation. On the other hand, graphitic carbon hardly affects the rate of formation of higher hydrocarbons, while on average longer hydrocarbons are obtained.

Figure 5c,d illustrates the strong impact of graphitic carbon on the paraffin to olefin ratio. At 260 °C, its presence suppresses the formation of C_2H_6 and C_3H_8 and slightly increases the formation of C_2H_4 and C_3H_6. Notably, the C_2H_6/C_2H_4 and C_3H_8/C_3H_6 ratios decrease by more than 95%: i.e., from 13.7 and 0.89 to 0.94 and 0.099, respectively. These relative changes are quantitatively consistent with the relative decrease in the CH_4 yield (88%) and the loss of cobalt surface as determined by the amount of carbon deposited by the TPH experiment (>90%). A similar trend is observed for the experiments carried out at 220 °C (Figure 5d). Experimental[8,53] and theoretical[30] studies have shown that olefins are the primary products of the FT reaction. Paraffins are therefore mostly obtained by hydrogenation of the primary olefins.

In order to establish how the graphitic carbon influences CO coverage and the hydrogenation rate, we carried out SSITKA measurements at 260 °C. Figure 6 compares the resulting residence time and coverages of CO and CH_x. With increasing graphitic carbon content, the CO coverage decreases. There is a strong correlation between the decrease in CO coverage and the loss of cobalt surface area as determined by H_2 chemisorption. The longer CH_x residence time with increasing graphitic carbon content implies slower CH_x hydrogenation to CH_4. This can be the result of two factors: i.e., (i) a decrease in the H coverage and (ii) a decrease in the amount of surface sites that produce mainly CH_4.

Consequently, the results presented in this section demonstrate a different effect of graphitic carbon on the various reaction routes from synthesis gas to CH_4 and higher hydrocarbons. While CO conversion, CH_4 and CO_2 formation, and olefin hydrogenation are substantially inhibited by graphitic carbon, the rate of formation of C_{2+} hydrocarbons is hardly affected. The results imply that the reaction pathway from CO to CH_4 is suppressed to a larger degree by graphitic carbon in comparison to that of CO to higher hydrocarbons. While the yield of higher hydrocarbons only decreases slightly, the chain-growth probability substantially increases due to the

DOI: 10.1021/acscatal.7b03639
ACS Catal. XXXX, XXX, XXX−XXX

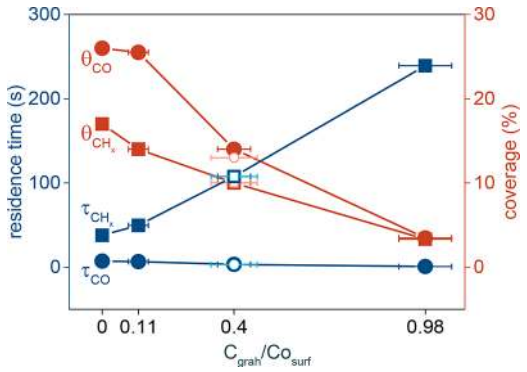

Figure 6. Residence times (blue) and coverages (red) of CH_x (squares) and CO (circles) as determined by SSITKA over carbon-precovered Co/SiO_2 catalysts as a function of C_{graph}/Co_{surf} (conditions: ρ_{H_2} = 200 mbar, ρ_{CO} = 200 mbar, T = 260 °C). The error bars present the systematic error introduced by the carbon quantification that is done by integrating the TPH profiles on a calibrated online MS.

presence of graphitic carbon. Before discussing these results in more detail, we will demonstrate that graphitic carbon species also slowly build up on an initially clean cobalt surface during CO hydrogenation and affect the catalytic performance in a manner similar to that shown in this section.

3.3. Influence of Carbon Deposits Formed during the FT Reaction. To study the buildup of carbon deposits during CO hydrogenation, we carried out model FT reaction experiments at H_2/CO ratios of 1 and 2 at 220 and 260 °C. Quantification of the carbon deposits by integrating the TPH profiles of spent catalysts allows establishing the correlation between carbon deposition and catalytic performance. In this case, we removed a significant part of the amorphous carbon in a H_2 flow at the reaction temperature for 6 h. Thereafter, the content of graphitic carbon on spent catalysts can be quantified by TPH.

As shown in Table 2, the amount of graphitic carbon increases with time on stream of the FT reaction. Figure 7a shows that the CO consumption rate at 260 °C decreases much more quickly with time on stream in comparison to that at 220 °C, while the effects are also less pronounced at a H_2/CO ratio of 2. This difference can be explained by the larger amount of graphitic carbon deposited at higher temperature and lower H_2/CO ratio.[54] Accordingly, we propose that the initial decrease in the CO consumption rate can be assigned to carbon deposition. Notably, there are also differences in the reactivity of the deposited graphitic carbon. Typically, the amount of graphitic carbon increases with the reaction temperature. We highlight the effect of the graphitic carbon buildup on the CH_4 and C_{2+} hydrocarbon yields in Figure 7b. These data are normalized to the initial values. In all cases, the CH_4 yields decrease much more quickly than the C_{2+} hydrocarbon yields and the effect is most pronounced at 260 °C and at low H_2/CO ratio.

Table 2. In Situ Formed Graphitic Carbon Content on Spent Cobalt Catalysts upon Different Experimental Procedures

temp (°C)	ρ_{CO} (mbar)	ρ_{H_2} (mbar)	TOS (h)	C_{graph}/Co_{surf}[a]
220	200	400	45	0.09
220	200	200	45	0.35
260	200	400	45	0.43
260	200	200	5	0.26
260	200	200	15	0.48
260	200	200	45	0.91

[a] C_{graph}/Co_{surf} determined by integration of the CH_4 signal above 260 °C during TPH (cf. Figure 1).

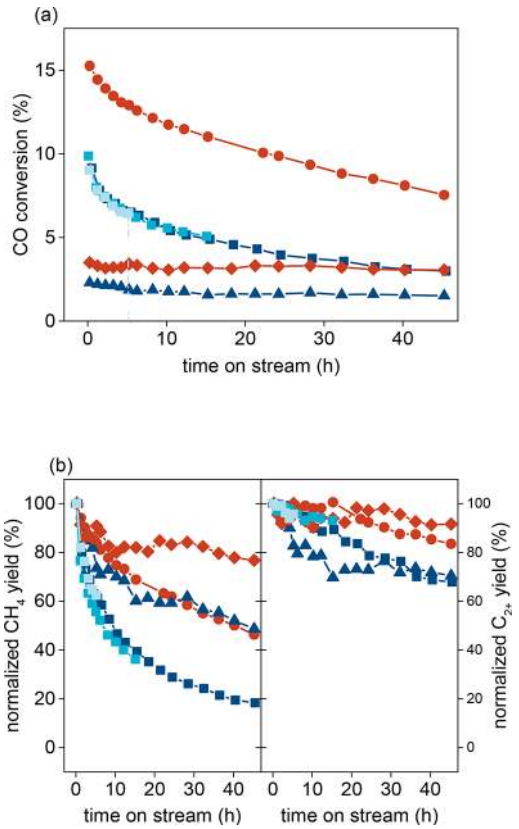

Figure 7. Evolution of (a) CO conversion and (b) normalized C_1 yield (left panel) and C_{2+} yield (right panel) as a function of time on stream under various conditions: (blue squares) ρ_{H_2} = 200 mbar, ρ_{CO} = 200 mbar, T = 260 °C; (red circles) ρ_{H_2} = 400 mbar, ρ_{CO} = 200 mbar, T = 260 °C; (blue triangles) ρ_{H_2} = 200 mbar, ρ_{CO} = 200 mbar, T = 220 °C; (red diamonds) ρ_{H_2} = 400 mbar, ρ_{CO} = 200 mbar, T = 220 °C. The lighter blue markers represent experiments run for 5, 15, and 45 h under the same conditions.

Figure 8 shows the evolution of the selectivity from C_1 to C_6 and the corresponding chain-growth probability obtained at 260 °C and a H_2/CO ratio of 1 with time on stream, reflecting the effect of graphitic carbon buildup during the reaction. Clearly, the CH_4 selectivity decreases substantially, while the influence on the C_{2+} hydrocarbon yield is much less pronounced. At the same time, the yield of higher hydrocarbons increases with the ongoing reaction. Another remarkable observation is that the selectivity of longer hydrocarbons increases more pronouncedly than the selectivity of shorter hydrocarbons, fully consistent with the increasing chain-growth probability. Finally, we plot the relative decrease in product yields with respect to the initial values as a function of the C_{graph}/Co_{surf} ratio in Figure 9. The decrease in CH_4 yield is strongly correlated with the graphitic carbon coverage. In contrast, the correlation of the C_{2+} hydrocarbon yield with the graphitic carbon coverage is much weaker.

DOI: 10.1021/acscatal.7b03639
ACS Catal. XXXX, XXX, XXX−XXX

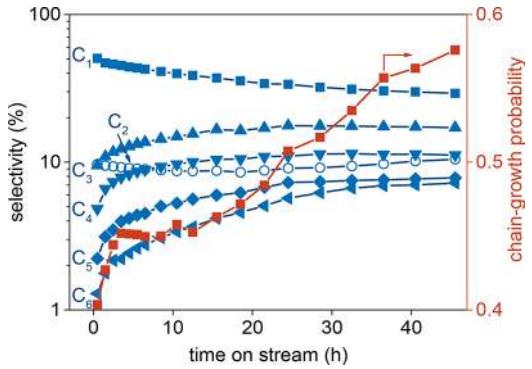

Figure 8. Evolution of selectivity and chain-growth probability (based on C_3−C_6 hydrocarbons) with time on stream (conditions: ρ_{H_2} = 200 mbar, ρ_{CO} = 200 mbar, T = 260 °C).

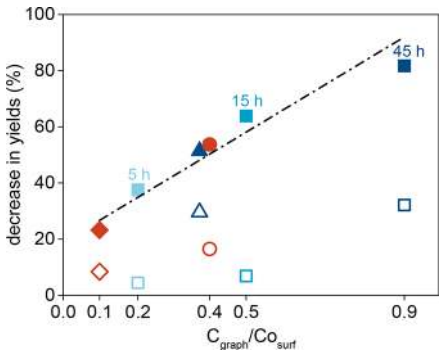

Figure 9. Relative decrease in CH_4 (solid symbols) and C_{2+} hydrocarbons (open symbols) yield with respect to initial values as a function of the C_{graph}/Co_{surf} ratio under various conditions: (squares) ρ_{H_2} = 200 mbar, ρ_{CO} = 200 mbar, T = 260 °C; (circles) ρ_{H_2} = 400 mbar, ρ_{CO} = 200 mbar, T = 260 °C; (triangles) ρ_{H_2} = 200 mbar, ρ_{CO} = 200 mbar, T = 220 °C; (diamonds) ρ_{H_2} = 400 mbar, ρ_{CO} = 200 mbar, T = 220 °C. The light blue squares represent experiments run for 5, 15, and 45 h under similar conditions. The line is a guide to the eye.

3.4. Influence of Carbon Deposits on Chain Growth.

In order to understand how chain growth is influenced by graphitic carbon, we studied the conversion of a C_3H_6/H_2 mixture on freshly reduced and carbon-covered cobalt catalysts. In an earlier work, we coreacted $^{13}CO/H_2$ synthesis gas with $^{12}C_3H_6$ to investigate the reversibility of chain growth and the inclusion of carbon species resulting from C−C bond cleavage reactions in propene into higher hydrocarbons.[55] Here, we did not use CO as a reactant in order to exclude any influence of CO coverage.[55] The cobalt catalyst containing graphitic carbon was prepared by ^{13}CO exposure at 260 °C for 30 min followed by H_2 exposure at 260 °C for 30 min. By using labeled ^{13}CO for deposition, we can track the origin of the carbon atoms in the hydrocarbon products in subsequent C_3H_6/H_2 reaction experiments. C_3H_6 is completely converted in these experiments, and C_3H_8 is the major product for both cases. The other products are hydrocarbons lighter and heavier than C_3 hydrocarbons. The selectivity results are collected in Figure 10 in the form of a plot of the logarithmic molar fraction as a function of the carbon number (ASF plot). These data demonstrate that the product distribution obtained from a C_3H_6/H_2 mixture is qualitatively similar to the typical ASF-type product distribution obtained with synthesis gas.[55] Figure 10 shows a lower CH_4 selectivity for the catalysts that contain graphitic carbon, consistent with the lower hydrogenation activity of the carbon-covered catalyst. At the same time, the chain-growth probability based on the C_4−C_7 hydrocarbon products increases from 0.23 for the initially clean cobalt catalyst to 0.42 for the cobalt catalyst that was precovered with graphitic carbon. These results are qualitatively in good agreement with the changes in the chain-growth probability due to the presence of graphitic carbon during the FT reaction. Isotopic analysis by GC-MS shows that the ^{13}C content in the hydrocarbon products is lower than 0.2%, confirming that the predeposited graphitic carbon species are not involved in the chain-growth reactions.

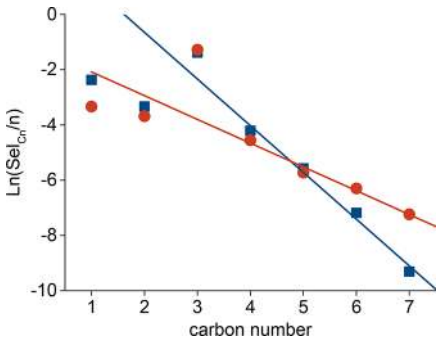

Figure 10. Anderson−Schulz−Flory plot of the products of the reaction of a C_3H_6/H_2 mixture on a clean (squares) and graphitic carbon precovered cobalt catalyst (circles) prepared by ^{13}CO exposure at 260 °C for 30 min followed by H_2 exposure at 260 °C for 2 h. C_3 products were excluded from the selectivity calculations (conditions: T = 220 °C, ρ_{H_2} = 600 mbar, $\rho_{C_3H_6}$ = 60 mbar).

4. DISCUSSION

The detailed mechanism of the FT reaction is far from understood. The FT reaction involves many elementary reaction steps, some of which are structure sensitive while others are expected to not depend significantly on the surface topology. Identifying how blocking of part of the catalyst surface affects activity and selectivity may provide deeper insight into the reaction mechanism and site requirements. In this study, we investigated how carbon deposits on the cobalt surface affect the CO consumption rate and the product distribution of the FT reaction.

By using the Boudouard reaction to cover a substantial part of the metallic surface by graphitic carbon, we demonstrate that the catalytic surface contains different sites involved in the production of CH_4 and higher hydrocarbons. The cobalt catalyst used contains ~15 nm particles. This size is larger than the minimum size of 6 nm, below which the catalytic performance is strongly dependent on particle size.[56,57] The surface of the nanoparticles in the present work will predominantly contain low-reactive planar surfaces, while about 20% of the surface will be made up of defects in the form of corners, edges, and step edges.[58] By combining $^{12}C^{16}O/^{13}C^{18}O$ isotopic scrambling with in situ infrared spectroscopy, we have demonstrated earlier that direct CO dissociation proceeds predominantly on step-edge sites.[37] This is consistent with the expected strong structure sensitivity of the CO dissociation reaction.

The main observation made in this work is that CH_4 and CO_2 formation rates and the paraffin to olefin ratio are substantially suppressed by the presence of graphitic carbon,

DOI: 10.1021/acscatal.7b03639
ACS Catal. XXXX, XXX, XXX−XXX

while the rate of higher hydrocarbon formation hardly changes. This result cannot be explained by assuming a surface that contains only one type of site, as one would expect a decrease in CO conversion without changes in selectivity. Accordingly, we discuss these findings in the framework of a surface that contains both step edge and terraces, as typically assumed in cobalt-catalyzed FT synthesis.[32,50,59] Our data show a very strong correlation among the CH_4 selectivity, the paraffin to olefin ratio, and the available cobalt surface, even for a catalyst in which more than 90% of the available cobalt sites were covered by graphitic carbon. Thus, we infer that a large part of CH_4 originates from CH_x hydrogenation on terrace sites, which is in keeping with the notion that CH_x hydrogenation to CH_4 is not a structure-sensitive reaction.[14] The observation of significantly inhibited olefin hydrogenation lines up with the dependence of CH_4 formation rate on graphitic carbon content. The observation that the yield of C_{2+} hydrocarbons is less affected is in keeping with the proposal that olefins are the primary product of the FT reaction.[8,30,53] Thus, the terraces are responsible for the hydrogenation of the primary olefin products, which is a structure-insensitive reaction as well. Similarly, the CO_2 yield correlates with the CH_4 yield, identifying the terrace surfaces as the major source of CO_2 formation. In contrast, the C_{2+} hydrocarbon formation rate changes only slightly when more than 90% of the surface is blocked. We therefore conclude that higher hydrocarbon formation occurs on a small fraction of the surface sites, which are most likely step-edge sites.[15,58] Although the C_{2+} hydrocarbon formation rate is hardly affected by graphitic carbon, the chain-growth probability is increased. This is in line with prolonged CH_x residence time, implying that more CH_x species can be built into growing chains. Altogether, our data are consistent with the view that CO dissociation and chain-growth reactions are structure sensitive and preferred on step-edge sites,[29,32] while hydrogenation and oxidation occur on the whole surface.[14,15]

An important aspect to be considered is the migration of surface adsorbates between the different types of surface sites. On the basis of the strong correlation between cobalt surface area and CH_4 formation rate, we speculate that the terrace sites are the origin of a large part of the production of CH_4. If we exclude migration of CH_x species from step-edge to terrace sites, CO dissociation leading to CH_4 must take place on the terrace sites. CO dissociation with assistance of adsorbed H on planar sites has been extensively discussed as an alternative to direct CO dissociation on step edges.[22−27] DFT calculations show that the H-assisted CO dissociation on terrace sites is feasible,[24,27] although the activation barrier is higher than on step-edge sites.[22] We refer to the work of Iglesia,[23,26,27] who proposed that the FT reaction exclusively takes place on cobalt terrace sites. However, this view cannot explain the distinct dependence of CH_4 and C_{2+} formation rates on carbon deposits, as well as the increase in chain-growth probability. Following this one-site model, one would not expect any change in selectivity when the catalyst surface is partially covered. We therefore also consider that H-assisted CO dissociation occurs on terrace sites, which mainly leads to CH_4, while CO dissociation taking place on step-edge sites leads to C_{2+} hydrocarbons and a small amount of CH_4. In other words, we cannot exclude that two parallel reaction pathways exist on terraces and steps. This thought provides an explanation for the decreased CO consumption rate in the presence of graphitic carbon. Notably, the CO consumption rate decreases with increasing graphitic carbon content, but not proportionally with the loss of cobalt surface area nor with the CO coverage or with the CH_4 formation rate. This is because the contribution of CO consumption via CO dissociation on step-edge sites is less affected by graphitic carbon in comparison to the route on terraces.

We provide an alternative scenario taking into account the migration of surface adsorbates between step-edge and terrace sites. We contrast the previous case by assuming that CO dissociation exclusively occurs at step edges. Then, C and O fragments obtained by CO dissociation can diffuse from the step edges to the terrace sites. C will be converted to mainly CH_4, because chain growth is not favorable on terrace sites.[15,32] At a low H_2/CO ratio, a fraction of these C atoms will be converted to graphitic carbon, as we observed in the present work, causing deactivation.[54] Similarly, O migrating to terraces will be converted to CO_2 due to the high CO coverage. Graphitic carbon on terrace sites will suppress CH_4 and CO_2 formation, in line with our experimental observations. Our earlier work shows that the CO consumption rate under methanation conditions is mainly limited by CH_x hydrogenation, meaning that suppression of CH_4 formation will cause a corresponding decrease in CO conversion. It also implies that blocking terrace sites slows CH_x hydrogenation to CH_4, thereby increasing the residence time of CH_x fragments. Thus, the CH_x fragment will reside longer on step-edge sites, resulting in a higher chain-growth probability. The higher coverage at the step-edge sites also suppresses cleavage of the growing hydrocarbon chains.[55] This view is also consistent with the C_3H_6/H_2 reaction experiments (Figure 10), in which C−C coupling is facilitated by the presence of graphitic carbon on terraces, since (i) CH_x migration to terraces is suppressed and (ii) higher CH_x coverage on step-edge sites suppresses C−C cleavage. Of equal importance is then the observation that the presence of graphitic carbon during C_3H_6/H_2 conversion decreases the CH_4 selectivity. This directly proves that C species formed at step edges can migrate to terrace sites and that graphitic carbon suppresses this migration. We propose that H-assisted CO dissociation on terraces can play a role in the overall CO consumption, but it will mainly lead to CH_4. Indeed, if C species originating from terrace sites would be involved in chain growth on step edges via migration, one would expect the C_{2+} hydrocarbons yield to decrease due to graphitic carbon. Therefore, this scenario can be excluded.

Our approach to selectively poison the surface with graphitic carbon provides new insight into the structure sensitivity of the FT reaction. Specifically, we have demonstrated that step-edge sites are the main active sites for the FT reaction. Graphitic carbon can slowly build up on terrace sites during CO hydrogenation. The buildup of such graphitic carbon occurs more quickly at higher temperature and lower H_2/CO ratio. On the time scale of our reaction (45 h), it is observed that a considerable amount of graphitic carbon is deposited at 260 °C. Under more typical FT conditions (T = 220 °C; H_2/CO = 2), the buildup is much slower. The in situ produced graphitic carbon has an effect similar to that of predeposited graphitic carbon. Figure 9 shows that the decrease in CH_4 selectivity strongly correlates with the graphitic carbon content. The decrease in the C_{2+} hydrocarbon yield is very low and is only substantial when nearly the complete surface is poisoned.

In this respect, it is important to emphasize again that CH_4 selectivity is an important parameter in practical FT technology.[7,8,11] Our data show that formation of non-ASF

DOI: 10.1021/acscatal.7b03639
ACS Catal. XXXX, XXX, XXX−XXX

CH_4 can be attributed to the structure sensitivity of the FT reaction. For instance, Figure 11 confirms the formation of

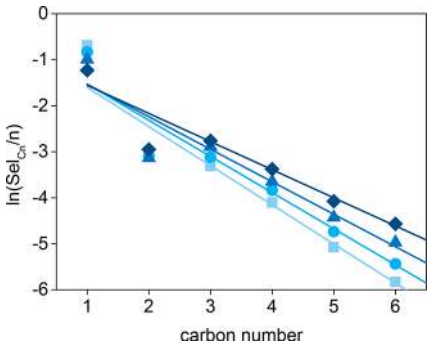

Figure 11. ASF distribution determined after 1 h (squares), 5 h (circles), 15 h (triangles), and 45 h (diamonds) time on stream (conditions: ρ_{H_2} = 200 mbar, ρ_{CO} = 200 mbar, T = 260 °C).

non-ASF CH_4 and its decrease with an increasing amount of graphitic carbon. It is also consistent with the microkinetics simulations carried out for stepped Ru in which a lower than ASF-predicted CH_4 selectivity is found.[30] In this respect, it is worthwhile to cite two computational works that have involved different surface sites in predicting cobalt catalytic performance.[59,60] Liu et al. studied the chain-growth mechanism on a Co($10\bar{1}1$) surface. Their results confirm that the stepped surface exhibits good selectivity toward C_{2+} hydrocarbons,[60] which is consistent with our observation that a small fraction of surface sites is responsible for higher hydrocarbon formation. Van Helden et al. explored a combination of step-edge sites for CO dissociation and terrace sites for chain growth using first-principles kinetic parameters obtained for cobalt surfaces.[59] The reactions assigned to the different surface sites in van Helden's studies are not consistent with our experimental observations.

Finally, we contrast the above interpretation with two important works on the FT reaction. Schulz has also discussed considerable changes in the CO conversion and product distribution for supported cobalt under typical FT conditions.[8,61,62] Notably, he observed an increasing olefin to paraffin ratio and chain-growth probability and decreasing CH_4 selectivity during the initial stages for a cobalt−rhenium catalyst. This is qualitatively similar to our observations. Schulz attributed these changes in part to the buildup of CO on planar sites, which for longer reaction times caused surface reconstruction.[61] This surface reconstruction led to an increase in the fraction of step-edge sites on the catalyst surface. Another relevant study was recently reported by Ralston et al.,[63] who observed that large cobalt particles (9.5 nm) contain more reactive carbon species and catalyze chain growth more effectively than small particles (4.3 nm). This observation is quantitatively consistent with the fraction of B_5−B sites, a certain type of step-edge site.[20,21,58,64] Therefore, the different performance for small and large particles was attributed to the density of step-edge sites. This conclusion is qualitatively in line with our work, as the balance between step-edge sites responsible for CO dissociation and chain propagation and terrace sites for CH_4 formation will determine the product distribution.

5. CONCLUSIONS

The influence of graphitic carbon on the FT reaction was investigated in detail. Carbon was deposited by the Boudouard reaction, which involves CO dissociation on step-edge sites, diffusion of C atoms to terrace sites, and agglomeration of these C atoms. On the basis of TPH, amorphous and graphitic carbon can be distinguished. Amorphous carbon can be hydrogenated below 260 °C, while graphitic carbon can only be removed by hydrogenation at much higher temperature. Consistent with the low temperature at which amorphous carbon can be removed, it does not influence the FT catalytic performance. The presence of predeposited graphitic carbon, on the other hand, has a profound influence on CO conversion and the product distribution. While CO conversion and CH_4 formation rate decrease, the formation rate of higher hydrocarbon is nearly unaffected by the presence of graphitic carbon. Additional FT experiments designed to study the effect of in situ formed carbon deposits led to the insight that slow buildup of graphitic carbon has similar effects in comparison to the predeposition of graphitic carbon. The formation of graphitic carbon is more pronounced at higher temperature and at lower H_2/CO ratio. We observe that the products of the H_2/C_3H_6 reaction follow the typical ASF-type product distribution of the FT reaction. The presence of graphic carbon using ^{13}CO facilitates C−C coupling reactions in terms of chain-growth probability, when the Co/SiO_2 catalyst is exposed to a C_3H_6/H_2 mixture. Considering the structure sensitivity of the various elementary reaction steps underlying the FT reaction, we reach the conclusion that two sites must be involved in the FT reaction. Step-edge sites catalyze CO dissociation and chain growth. CH_x species formed on step-edge sites are involved in chain growth and CH_4 formation on step-edge sites and can also diffuse to terrace sites, where they are predominantly hydrogenated to CH_4. The terrace sites favor methanation, thereby explaining the occurrence of non-ASF CH_4. Under particular conditions, graphitic carbon can build up on terrace sites, therefore decreasing non-ASF CH_4. We emphasize that this new understanding about the origin of non-ASF CH_4 in the FT reaction can help to design improved catalysts. By selectively blocking only the methanation sites and not CO dissociation and chain growth sites, we believe that a decrease in methane selectivity can be achieved without much loss in activity toward higher hydrocarbons.

AUTHOR INFORMATION

Corresponding Author

*E-mail for E.J.M.H.: e.j.m.hensen@tue.nl.

ORCID

Emiel J. M. Hensen: 0000-0002-9754-2417

Notes

The authors declare no competing financial interest.

ACKNOWLEDGMENTS

The authors are grateful to M.Sc. Andrey Goryachev for providing the highly oriented pyrolytic graphite reference used in C 1s spectra fitting.

REFERENCES

(1) Fischer, F.; Tropsch, H. *Brennst. Chem.* **1926**, *7*, 97−104.
(2) Fischer, F.; Tropsch, H. *Brennst. Chem.* **1930**, *11*, 489−500.
(3) Stranges, A. N. *Stud. Surf. Sci. Catal.* **2007**, *163*, 1−27.
(4) Schulz, H. *Appl. Catal., A* **1999**, *186*, 3−12.

DOI: 10.1021/acscatal.7b03639
ACS Catal. XXXX, XXX, XXX−XXX

(5) Dry, M. E. *Appl. Catal., A* **1996**, *138*, 319−344.
(6) Dry, M. E. *Catal. Today* **1990**, *6*, 183−206.
(7) Dry, M. E. *Catal. Today* **2002**, *71*, 227−241.
(8) Schulz, H. *Top. Catal.* **2003**, *26*, 73−85.
(9) Henrici-Olivé, G.; Olivé, S. *Angew. Chem., Int. Ed. Engl.* **1976**, *15*, 136−141.
(10) Pichler, V. H.; Schulz, H.; Elstner, M. *Brennst. Chem.* **1967**, *48*, 78−87.
(11) Schulz, H. *Catal. Today* **2013**, *214*, 140−151.
(12) Markvoort, A. J.; van Santen, R. A.; Hilbers, P. A.; Hensen, E. J. *Angew. Chem., Int. Ed.* **2012**, *51*, 9015−9019.
(13) Prieto, G.; De Mello, M. I. S.; Concepción, P.; Murciano, R.; Pergher, S. B. C.; Martínez, A. n. *ACS Catal.* **2015**, *5*, 3323−3335.
(14) Liu, Z.-P.; Hu, P. *J. Am. Chem. Soc.* **2003**, *125*, 1958−1967.
(15) van Santen, R. A. *Acc. Chem. Res.* **2009**, *42*, 57−66.
(16) Ciobica, I. M.; van Santen, R. A. *J. Phys. Chem. B* **2003**, *107*, 3808−3812.
(17) Ge, Q.; Neurock, M. *J. Phys. Chem. B* **2006**, *110*, 15368−15380.
(18) Hammer, B. *Phys. Rev. Lett.* **1999**, *83*, 3681−3684.
(19) Rempel, J.; Greeley, J.; Hansen, L. B.; Nielsen, O. H.; Nørskov, J. K.; Mavrikakis, M. *J. Phys. Chem. C* **2009**, *113*, 20623−20631.
(20) Dahl, S.; Logadottir, A.; Egeberg, R. C.; Larsen, J. H.; Chorkendorff, I.; Törnqvist, E.; Nørskov, J. K. *Phys. Rev. Lett.* **1999**, *83*, 1814−1817.
(21) Honkala, K.; Hellman, A.; Remediakis, I. N.; Logadottir, A.; Carlsson, A.; Dahl, S.; Christensen, C. H.; Norskov, J. K. *Science* **2005**, *307*, 555−558.
(22) Shetty, S.; Jansen, A. P. J.; van Santen, R. A. *J. Am. Chem. Soc.* **2009**, *131*, 12874−12875.
(23) Hibbitts, D.; Iglesia, E. *Acc. Chem. Res.* **2015**, *48*, 1254−1262.
(24) Mitchell, W. J.; Xie, J.; Jachimowski, T. A.; Weinberg, W. H. *J. Am. Chem. Soc.* **1995**, *117*, 2606−2617.
(25) Huo, C.-F.; Li, Y. W.; Wang, J.; Jiao, H. *J. Phys. Chem. C* **2008**, *112*, 14108−14116.
(26) Ojeda, M.; Nabar, R.; Nilekar, A. U.; Ishikawa, A.; Mavrikakis, M.; Iglesia, E. *J. Catal.* **2010**, *272*, 287−297.
(27) Loveless, B. T.; Buda, C.; Neurock, M.; Iglesia, E. *J. Am. Chem. Soc.* **2013**, *135*, 6107−6121.
(28) Cheng, J.; Hu, P.; Ellis, P.; French, S.; Kelly, G.; Lok, C. M. *J. Phys. Chem. C* **2008**, *112*, 6082−6086.
(29) van Santen, R. A.; Ciobîcă, I. M.; van Steen, E.; Ghouri, M. M. *Adv. Catal.* **2011**, *54*, 127−187.
(30) Filot, I. A. W.; van Santen, R. A.; Hensen, E. J. M. *Angew. Chem., Int. Ed.* **2014**, *53*, 12746−12750.
(31) Moodley, D. J.; van de Loosdrecht, J.; Saib, A. M.; Overett, M. J.; Datye, A. K.; Niemantsverdriet, J. W. *Appl. Catal., A* **2009**, *354*, 102−110.
(32) Cheng, J.; Gong, X.; Hu, P.; Lok, C.; Ellis, P.; French, S. *J. Catal.* **2008**, *254*, 285−295.
(33) Nakamura, J.; Tanaka, K.-i.; Toyoshima, I. *J. Catal.* **1987**, *108*, 55−62.
(34) Nakamura, J.; Toyoshima, I.; Tanaka, K.-i. *Surf. Sci.* **1988**, *201*, 185−194.
(35) Lee, D.-K.; Lee, J.-H.; Ihm, S.-K. *Appl. Catal.* **1988**, *36*, 199−207.
(36) Weststrate, C. J.; Kızılkaya, A. C.; Rossen, E. T. R.; Verhoeven, M. W. G. M.; Ciobîcă, I. M.; Saib, A. M.; Niemantsverdriet, J. W. *J. Phys. Chem. C* **2012**, *116*, 11575−11583.
(37) Chen, W.; Zijlstra, B.; Filot, I. A. W.; Pestman, R.; Hensen, E. J. M. *ChemCatChem* **2017**, DOI: 10.1002/cctc.201701203.
(38) Chen, W.; Pestman, R.; Zijlstra, B.; Filot, I. A. W.; Hensen, E. J. M. *ACS Catal.* **2017**, *7*, 8050−8060.
(39) McCarty, J. G.; Wise, H. *J. Catal.* **1979**, *57*, 406−416.
(40) Fei Tan, K.; Xu, J.; Chang, J.; Borgna, A.; Saeys, M. *J. Catal.* **2010**, *274*, 121−129.
(41) Blume, R.; Rosenthal, D.; Tessonnier, J.-P.; Li, H.; Knop-Gericke, A.; Schlögl, R. *ChemCatChem* **2015**, *7*, 2871−2881.
(42) Swart, J. C. W.; Ciobîcă, I. M.; van Santen, R. A.; van Steen, E. *J. Phys. Chem. C* **2008**, *112*, 12899−12904.
(43) Böller, B.; Ehrensperger, M.; Wintterlin, J. *ACS Catal.* **2015**, *5*, 6802−6806.
(44) Wu, C. H.; Eren, B.; Bluhm, H.; Salmeron, M. B. *ACS Catal.* **2017**, *7*, 1150−1157.
(45) Biesinger, M. C.; Payne, B. P.; Grosvenor, A. P.; Lau, L. W. M.; Gerson, A. R.; Smart, R. S. C. *Appl. Surf. Sci.* **2011**, *257*, 2717−2730.
(46) Farr, N. G.; Griesser, H. J. *J. Electron Spectrosc. Relat. Phenom.* **1989**, *49*, 293−302.
(47) Ye, D. X.; Pimanpang, S.; Jezewski, C.; Tang, F.; Senkevich, J. J.; Wang, G. C.; Lu, T. M. *Thin Solid Films* **2005**, *485*, 95−100.
(48) Rodriguez-Gomez, A.; Holgado, J. P.; Caballero, A. *ACS Catal.* **2017**, *7*, 5243−5247.
(49) Bremmer, G. M.; Zacharaki, E.; Sjastad, A. O.; Navarro, V.; Frenken, J. W. M.; Kooyman, P. J. *Faraday Discuss.* **2017**, *197*, 337−351.
(50) Liu, J.-X.; Su, H.-Y.; Li, W.-X. *Catal. Today* **2013**, *215*, 36−42.
(51) Shetty, S.; van Santen, R. A. *Catal. Today* **2011**, *171*, 168−173.
(52) Joos, L.; Filot, I. A. W.; Cottenier, S.; Hensen, E. J. M.; Waroquier, M.; Van Speybroeck, V.; van Santen, R. A. *J. Phys. Chem. C* **2014**, *118*, 5317−5327.
(53) Friedel, R. A.; Anderson, R. B. *J. Am. Chem. Soc.* **1950**, *72*, 1212−1215.
(54) Keyvanloo, K.; Fisher, M. J.; Hecker, W. C.; Lancee, R. J.; Jacobs, G.; Bartholomew, C. H. *J. Catal.* **2015**, *327*, 33−47.
(55) Chen, W.; Filot, I. A. W.; Pestman, R.; Hensen, E. J. M. *ACS Catal.* **2017**, *7*, 8061−8071.
(56) Bezemer, G. L.; Bitter, J. H.; Kuipers, H. P. C. E.; Oosterbeek, H.; Holewijn, J. E.; Xu, X.; Kapteijn, F.; van Dillen, A. J.; de Jong, K. P. *J. Am. Chem. Soc.* **2006**, *128*, 3956−3964.
(57) den Breejen, J. P.; Radstake, P. B.; Bezemer, G. L.; Bitter, J. H.; Frøseth, V.; Holmen, A.; Jong, K. P. d. *J. Am. Chem. Soc.* **2009**, *131*, 7197−7203.
(58) van Helden, P.; Ciobîcă, I. M.; Coetzer, R. L. J. *Catal. Today* **2016**, *261*, 48−59.
(59) van Helden, P.; Berg, J.-A. v. d.; Petersen, M. A.; Janse van Rensburg, W.; Ciobica, I. M.; van de Loosdrecht, J. *Faraday Discuss.* **2017**, *197*, 117−151.
(60) Liu, H.; Zhang, R.; Ling, L.; Wang, Q.; Wang, B.; Li, D. *Catal. Sci. Technol.* **2017**, *7*, 3758−3776.
(61) Schulz, H.; Nie, Z.; Ousmanov, F. *Catal. Today* **2002**, *71*, 351−360.
(62) Schulz, H.; Nie, Z.; Claeys, M. *Stud. Surf. Sci. Catal.* **1998**, *119*, 191−196.
(63) Ralston, W. T.; Melaet, G.; Saephan, T.; Somorjai, G. A. *Angew. Chem., Int. Ed.* **2017**, *56*, 7415−7419.
(64) van Hardeveld, R.; Hartog, F. *Surf. Sci.* **1969**, *15*, 189−230.

DOI: 10.1021/acscatal.7b03639
ACS Catal. XXXX, XXX, XXX−XXX